IEEE Access
Multidisciplinary | Rapid Review | Open Access Journal

Received 25 April 2024, accepted 9 May 2024, date of publication 15 May 2024, date of current version 30 May 2024.

Digital Object Identifier 10.1109/ACCESS.2024.3401467

RESEARCH ARTICLE

Performance Analysis of Reluctance Coil Launchers Driven by Distributed Feeder Circuit

MENGKUN LU[1], XIANGLIE YI[2], ZHIFANG YUAN[2], AND WEI GAO[2]
[1]School of Mechanical Engineering, Hubei Engineering University, Xiaogan 432000, China
[2]School of Electrical Engineering, Naval University of Engineering, Wuhan 430033, China

Corresponding author: Mengkun Lu (lumengkun666670@sina.com)

This work was supported in part by the National Natural Science Foundation of China under Grant 52107136.

ABSTRACT Reluctance coil launchers usually use a pulse current formed by capacitive discharge to excite the excitation coil when launching. The pulse current peaks are high, and the projectile usually undergoes deep magnetic saturation, resulting in low launching efficiency. To address this problem, this article proposes using distributed feeder circuit to drive reluctance coil launchers, replacing the traditional single set of large-capacity capacitor discharge scheme with multiple small-capacity capacitors discharged in a time-sequential manner, so as to reduce the peak current and suppress magnetic saturation problems. The study includes two main aspects, one is to study the effect of the driving method on the launch performance and analyze the reasons; the other is to propose the calculation of the time-varying data in the launch process by the time-segmented calculation method. The efficiency of the model described in the paper is only 1.301% when using a single high-capacity capacitor for launching, while the launching efficiency is increased to 3.535% when driven by the distributed feeder circuit, indicating that the method can effectively improve the launching performance.

INDEX TERMS Reluctance coil launcher, magnetic saturation, distributed feeder circuit, flat-topped wave current, time-segmented calculation method.

I. INTRODUCTION

Pulsed-current-driven electromagnetic launchers (EMLs) are mainly categorized into rail-type, coil-type and reconnection-type, etc. [1] and [2]. Reluctance coil launcher is one of the coil-type launchers, mainly characterized by a ferromagnetic projectile material [3], whose launching process is not only transient, but also very difficult to analyze due to the strong nonlinearity [4]. Compared to other types of EMLs, the advantages of reluctance coil launchers include small size, light weight, low drive current, no friction, low sound, and good controllability [5], [6]. Currently, reluctance coil launchers are still in the research phase, but a few applications that tend to be mature have emerged.

The main applications of reluctance coil launchers include: 1) Reluctance coil guns (RCG), which has the advantage of adjustable power compared to gunpowder firearms [7], [8] and also guarantees a higher rate of fire and stability compared to pneumatic firearms. 2) The split Hopkinson pressure bar (SHPB) device with EM loading method has many advantages over traditional pneumatic loading, such as low noise, high energy conversion rate, and easy miniaturization [9], [10]. 3) With the increasingly demanding requirements for riveting performance in high-precision manufacturing industries such as aircraft manufacturing, the research of electromagnetic (EM) riveting technology has been emerged [11]. Compared to induction type coil riveting gun, reluctance type EM ones in the riveting of small size rivets need to capacitance energy storage is reduced dramatically, the discharge current is also greatly reduced, has the advantages of small size, light weight, low heat, easy to operate, safer, and so on. Similar applications include EM presses, EM nail guns, EM pumps, EM hemming machines, etc. [12]. 4) B. Zhu et al. combined a reluctance coil launcher

The associate editor coordinating the review of this manuscript and approving it for publication was Kai-Da Xu.

with an orbital launcher to give it the advantages of a coil-type transmitter's structural symmetry, high energy conversion efficiency for low and medium-speed launches, and ease of launching large-mass loads, while at the same time offering the advantages of synchronized feeds from a rail-type launcher [13], realizing the complementary advantages of different EM launching principles. 5) As an actuator for the robot to output impact power, the accompanying robot designed by V. Gies et al. to simulate a soccer ball pushed by a human leg has the advantages of small size, light weight, and small swing space of the motion joints. Compared to linear motors, rotary motors with supporting actuators, pneumatic actuators and other mechanical structures that output the same instantaneous thrust, the reluctance coil launcher has the advantages of small size, light weight, and the advantages of small swing space of the motion joints [14].

Reluctance coil launchers are driven by high peak pulse currents and commonly suffer from magnetic saturation. Especially when the projectile mass is heavy and has to be driven with a higher launch energy at the beginning of the launch in order to overcome the inertial effect, the high peak pulse lasts for a longer time, when the projectile is deeply magnetically saturate [15], [16], resulting in low launch efficiency.

The launching efficiency of reluctance coil launcher is the ratio of the kinetic energy of the projectile to the electrical energy released by the capacitors. The values of single-stage reluctance coil launchers in existing studies are generally in the range of 0 to 15%, and decrease significantly when the muzzle velocity of the projectile is fast. There are many ways to improve the efficiency, such as reducing the air gap between the projectile and the coil, optimizing the design parameters, suppressing the reverse electromagnetic force (EMF) [17], etc., and it is necessary to apply a variety of methods in order to obtain a high total launch efficiency. In the existing studies, El-Hasan accelerated a projectile weighing 2.56 g to 212 m/s with an efficiency of 1.65% [18]. S.J. Lee et al. used a 0.1 F capacitor and 200 V discharge voltage to accelerate a 5.15 g projectile. The peak EMF on the projectile reached 15 kN, the peak current was about 5 kA, and the peak velocity of the projectile was 193 m/s. However, due to the reverse EMF, the actual efficiency was only 0.387% [19]. Leubner et al. used the designed RCG to accelerate a projectile weighing 19.6 g to 28.9 m/s with a launch efficiency of 1.88% [20]. Orbach et al. accelerated a projectile weighing 1.9 g to 54.3 m/s with an efficiency of 0.13 [21].

The methods and results of recent studies to enhance the efficiency of single-stage reluctance coil launcher are shown in Table 1. It should be noted that due to the numerous factors affecting efficiency, such as the manufacturing process determines the width of the air gap, which has a very pronounced effect on performance, and the experimental devices and parameters in the studies are not consistent, the horizontal comparison between efficiency is of no reference value.

In order to obtain a higher muzzle velocity, rail-type EM launchers often utilize a distributed feeder circuit to accelerate the armature, whose power supply circuit consists of multi-stage energy storage capacitors and inductors. The power supply circuit consists of multi-stage energy storage capacitors and inductors, and the role of inductors includes current limiting, isolating each discharge unit, regulating pulse width and intermediate energy storage, etc. [27] and [28]. Its various stages of pulse discharge units are triggered in time sequence to form a flat-topped pulsed excitation current to drive the armature. In contrast, reluctance coil launchers have a larger inductance and can form a flat-top current without the need for an additional inductor [29], [30], [31]. According to the driving principle, as long as there is current in the coil, regardless of whether the current fluctuates greatly or not, a magnetic field will be formed to drive the projectile, and thus a flat-top current drive can be used theoretically. Potential advantages of this driving method include the ability to limit the amplitude of the current with a certain amount of capacitive energy, thereby reducing magnetic saturation problems and enhancing the launch effect. The main difficulty in the calculation of this drive mode lies in the influence of the trigger time on the circuit at each stage, which must be accurately switched according to the on-time of the thyristor and the discharge state of the circuit to calculate the equation.

In view of this, the single large-capacity capacitor of the single-stage reluctance coil launcher is replaced by multiple small-capacity capacitors, which discharge in time order to drive the projectile. The focus of the research includes two aspects, one is to study the effect of this driving method on the launching performance and analyze the reasons; the other is to propose the basic calculation method for this launching process.

II. THE TIME-SEGMENTED CALCULATION METHOD

A. INTRODUCTION TO DISTRIBUTED FEEDER CIRCUIT

Single-stage reluctance coil launchers are typically driven using a pulsed discharge circuit with a crowbar diode, as shown in Fig. 1. When current is applied to the coil, a solenoidal magnetic field is formed and the projectile made of ferromagnetic material will be magnetized, according to the principle of minimum magnetoresistance, the projectile will move towards the center of the coil [32].

As shown in Fig. 1, although there may be stray inductance, resistance and capacitance in each branch of the pulse discharge circuit, in fact, because the experimental setup of the reluctance coil launcher is usually small in size, the influence of the stray resistance is the most obvious. The diode branch has fewer components, and the stray resistance can also be ignored, thus the most obvious influence on the launch performance is the stray resistance of the capacitor branch (including the on-resistance of the thyristor) and the total resistance of the coil branch (including the resistance of the coil).

TABLE 1. The methods and results of recent studies to enhance the efficiency of single-stage reluctance coil launcher.

Researcher	Methods of efficiency improvement	Mass of the projectile (g)	Material of the projectile	Muzzle velocity (m/s)	Pre-optimization efficiency (%)	Optimized efficiency (%)	Efficiency gains (%)
T. Barrera et al. [22]	The surface of the projectile is slotted to reduce the induced eddy current	30.475	Electrical iron (DT4C)	23.07	7.67	7.86	2.48
H. Deng et al. [3]	Replacement of projectile material from ferrite (PC40) to iron-colbat alloy	340	Iron-colbat alloy (1J27)	10.23	1.64	8.92	443.9
C. Liang et al. [17]	Circuit improvement to reduce the residual current in the coil	40	Steel Q235	20	3.74	7.43	98.7
H. Deng et al. [23]	Ditto	338	Electrical iron (DT4C)	113.34	5.25	5.75	9.52
J. Zhao et al. [24]	Circuit improvement for residual power recovery	153.89	Steel 20	13.67	4.37	5.89	34.78
M. M. M. Abdo et al. [25]	Installation of an iron shell outside the coil to increase the magnetic permeability	12.3	Medium carbon steel	14.9	2.6	2.78	6.92
V. Sari [26]	Installation of iron shells outside the coil, adjustment of projectile position, optimization of coil structure, etc.	36	Steel AISI1020	25.8	3.5	6.33	80.9

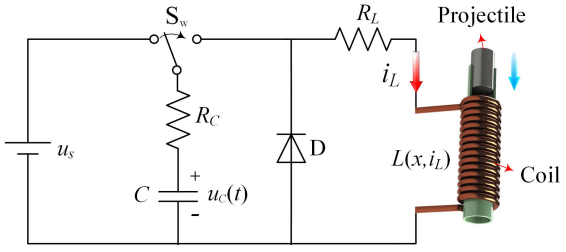

FIGURE 1. Common driving circuit for single-stage reluctance coil launchers.

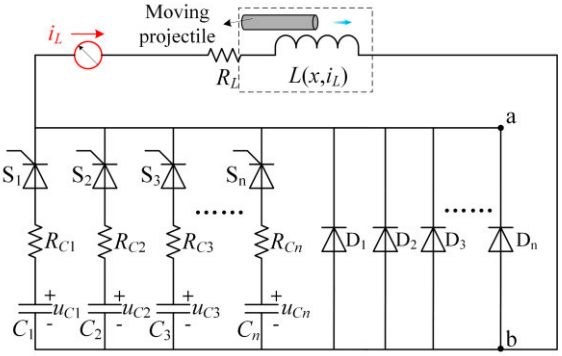

FIGURE 2. Schematic of the distributed feeder circuit used to drive single-stage reluctance coil launchers.

Due to the action of the crowbar diode D, the pulse current formed by the discharge of capacitor C should be derived in to resistor-inductor-capacitor (RLC) and resistor-inductor (RL) time segments [33]. Unlike pulsed circuits with constant inductance values, the projectile moves upward in the coil axis under the action of EMF during the launching process of the reluctance coil launcher, which affects the specific value of inductance and pulse current. At the same time the magnetic saturation problem makes the inductance vary nonlinearly, and thus the equivalent inductance is expressed in the calculation process as $L(x, i_L)$ and simultaneously solved by coupling the equations of motion [34]. As a result, the computational process is more complex and cannot obtain an analytical solution, which is more suitable for the derivation of the semi-analytical method or computation through the finite element method (FEM).

When the capacitor C has a large capacitance value, the peak pulse current is high and the projectile is prone to deep magnetic saturation resulting in low efficiency. Replace it with a distributed feeder circuit drive schematic of multiple small capacity capacitors discharged in a time-sequential order as shown in Fig. 2.

As shown in Fig. 2, due to the parallel connection of each pulse discharge unit, each diode terminal voltage is equal and together with the state on or off, that is, any capacitor to start discharging can make the voltage of the crowbar diode (u_{ab}) change, thereby changing the direction of current flow. We can calculate the time segment based on u_{ab} and the conduction time of each thyristor S to split the time segments for calculation, which is called time segmented calculation method in this paper.

B. CALCULATION EQUATIONS FOR THE 1ST STAGE WORKING ALONE

The entire launching process is analyzed by cutting the on-time of each thyristor into multiple time segments. The 1st stage working alone means that when each capacitor has energy storage, and only thyristor S_1 is switched on.

Let the current in the capacitor branch be i_C, the renewal current be i_D, the load current be i_L, The turn-on time of the n-stage thyristor is t_n, where the moment 0 represents the time at which the 1st stage thyristor conducts be t_n,

and the time at which the 1st stage of the crowbar diode conducts be t_{ab1}. The current in the excitation coil is first supplied by the *RLC* circuit (time condition $0 < t \leq t_{ab1}$), and an underdamped oscillation circuit is presented before the crowbar diode conducts, the current $i_C = i_L$, $i_D = 0$. From the law of KVL (Kirchhoff's Voltage Law)

$$u_C(t) = (R_{C1} + R_L)\, i_L + \frac{\mathrm{d}\psi}{\mathrm{d}t}. \tag{1}$$

For reluctance coil launchers, the magnetic chain ψ is a variable related to the coil current and the position of the thrower, so it should be expressed as

$$\psi(t) = L(x, i_L) \cdot i_L. \tag{2}$$

Since x and i_L are both time-dependent functions,

$$\frac{\mathrm{d}\psi}{\mathrm{d}t} = L(x, i_L) \cdot \frac{\mathrm{d}i_L}{\mathrm{d}t} + i_L \cdot \frac{\mathrm{d}L(x, i_L)}{\mathrm{d}t}. \tag{3}$$

Considering $i_L = -C\left(\mathrm{d}u_C/\mathrm{d}t\right)$ and substituting (3) into (1) yields the circuit equation for the *RLC* time segment as

$$u_{C1}(t) = -C_1\left(R_{C1} + R_L + \frac{\mathrm{d}L(x, i_L)}{\mathrm{d}t}\right)\frac{\mathrm{d}u_{C1}}{\mathrm{d}t} - C_1 L(x, i_L)\frac{\mathrm{d}^2 u_{C1}}{\mathrm{d}t^2}, \tag{4}$$

$$\frac{\mathrm{d}i_L}{\mathrm{d}t} = -C_1\frac{\mathrm{d}^2 u_{C1}}{\mathrm{d}t^2} = \frac{u_{C1} + C_1\left(R_{C1} + R_L + \frac{\mathrm{d}L(x,i_L)}{\mathrm{d}t}\right)\frac{\mathrm{d}u_{C1}}{\mathrm{d}t}}{L(x, i_L)}. \tag{5}$$

The voltage u_{ab} in the branch of the renewable diode can be expressed as

$$u_{ab}(t) = u_{C1} - R_{C1} i_{C1}. \tag{6}$$

Let $u_{ab}(t) = 0$ to obtain the time point at which the *RLC* circuit switches to the *RL* circuit t_{ab1} and its corresponding capacitor voltage $u_C(t_{ab1})$ and current $i_C(t_{ab1}) = I_{tab1}$.

When $u_{ab} \leq 0$ the pulse current is supplied by the *RL* circuit instead. After the crowbar diode conducts ($t > t_{ab1}$), the point in time at which the capacitor discharge ends ($u_C = 0$) lags behind the point in time at which the crowbar diode branch voltage $u_{ab} = 0$ is present due to the presence of the capacitor branch stray inductor resistance. Thus, the *RLC* circuit and the *RL* circuit operate simultaneously during this time segment, which can be analyzed using the principle of superposition, and the branch current $i_L = i_C + i_D$. According to KVL, where the voltage equation for the *RLC* circuit is

$$u_{C1}(t_{ab1}) = R_{C1} i_{C1} + R_L i_L + \frac{\mathrm{d}L(x, i_L)}{\mathrm{d}t} i_L + L(x, i_L)\frac{\mathrm{d}i_L}{\mathrm{d}t} + \frac{1}{C}\int_{t_{ab1}}^{t} i_{C1}\mathrm{d}t, \tag{7}$$

and *RLC* circuit is

$$0 = R_L i_L + \frac{d\psi}{\mathrm{d}t} = R_L i_L + L(x, i_L)\frac{\mathrm{d}i_L}{\mathrm{d}t} + \frac{\mathrm{d}L(x, i_L)}{\mathrm{d}t} i_L. \tag{8}$$

From (6), it can be seen that when u_{ab} decreasing to 0, not necessarily u_C reduced to 0. At this time

$$u_{C1}(t_{ab1}) - \frac{1}{C}\int_{t_{ab}}^{t} i_{C1}\mathrm{d}t = 0. \tag{9}$$

It can be seen that after the crowbar diode conduction, when there is still a residual voltage in the capacitor, the discharge process of the capacitor branch has nothing to do with the electrical parameters of the excitation coil branch, and the residual power in the capacitor is equivalent to the *RC* circuit is completely consumed, the circuit equation is

$$u_{C1}(t) = u_{C1}(t_{ab1})\, e^{-\frac{1}{R_{C1}C_1}(t - t_{ab1})}. \tag{10}$$

After the crowbar diode conduction ($t \geq t_{ab}$) for the *RL* renewal circuit time segment, from the (8) can be obtained in this time segment the current in the coil is

$$i_L(t) = -\int_{t_{ab1}}^{t}\left(\frac{\mathrm{d}L(x, i_L)}{\mathrm{d}t} + R_L\right)\cdot\frac{i_L}{L(x, i_L)}\mathrm{d}t + I_{tab1}. \tag{11}$$

During the *RL* renewal time segment, each diode equalizes the current in the excitation coil branch and each branch current is only $1/n$ of the coil branch current.

In summary, in time segment $0 \leq t < t_2$, the current in the excitation coil is calculated in two time segments according to (5) and (11) where the initial voltage $u_{C1}(0)$ of capacitor C_1 is integrated twice to (5) to establish the voltage equation.

C. CALCULATION EQUATIONS OF THE SUBSEQUENT STAGE

Let the 2nd stage thyristor S_2 conducts at the moment t_2. The calculation process can be analyzed in two cases.

1) SCENARIO 1: S_2 CONDUCTS WHEN $u_{ab} > 0$

If thyristor S_2 conducts when $u_{ab} > 0$. Capacitor C_1 discharge is not yet finished, the circuit is *RLC* time segment, then at this time the conduction of S_2 will not affect the diode's operating state, the two-stage pulse discharge unit are RLC circuit. According to the principle of circuit superposition it can be seen that $i_L = i_{C1} + i_{C2}$, the total excitation current is a simple superposition of the currents of the 1st and the 2nd *RLC* circuit stages, the circuit schematic is shown in Fig. 3.

Since there is $u_{ab} > 0$ at moment t_2, capacitor C_1 has not finished discharging, so it is still the *RLC* discharge time segment, the excitation current is

$$i_L(t) = \int_{t_2}^{t}\left(\begin{array}{l} u_{C1} + C_1\left(R_{C1} + R_L + \frac{\mathrm{d}L(x,i_L)}{\mathrm{d}t}\right)\frac{\mathrm{d}u_{C1}}{\mathrm{d}t} \\ +u_{C2} + \left(R_{C2} + R_L + \frac{\mathrm{d}L(x,i_L)}{\mathrm{d}t}\right)\frac{\mathrm{d}u_{C2}}{\mathrm{d}t} \end{array}\right) \times \frac{1}{L(x, i_L)}\mathrm{d}t. \tag{12}$$

In (12), the initial voltage value of the capacitor is $u_{C1}(t_2)$ and $u_{C2}(t_2)$ respectively, where $u_{C1}(t_2)$ is the residual

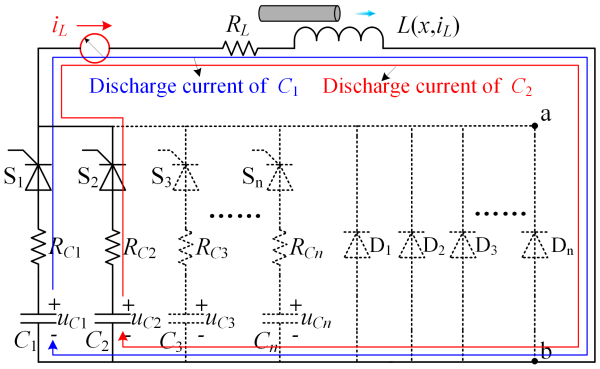

FIGURE 3. Current flow path in the first scenario.

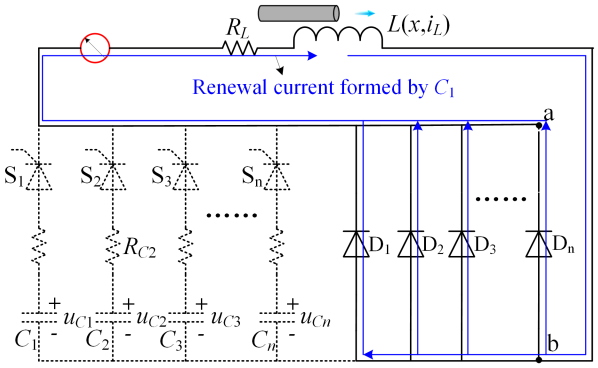

(a) The current flow direction before the moment t_2

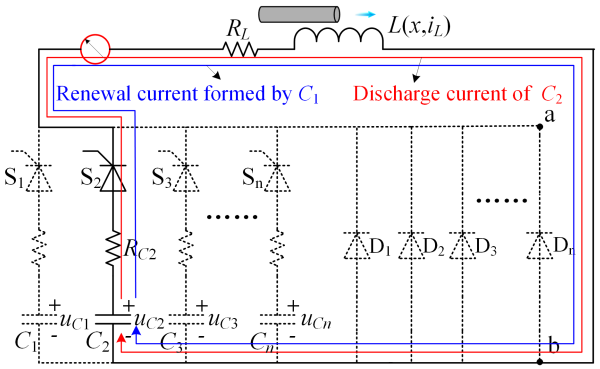

(b) The current flow direction after the moment t_2

FIGURE 4. Current flow path in the second scenario.

voltage after capacitor C_1 is discharged separately during segment $0 \leq t < t_2$, and $u_{C2}(t_2)$ is the initial charging voltage of capacitor C_2 before it starts discharging.

Since the thyristor has a unidirectional conduction characteristic, the positive terminal of C_1 will not be charged to form an equalizing voltage even if the voltage of capacitor C_2 is higher than that of capacitor C_1. It can be inferred that when multiple capacitors discharge at the same time, the conduction condition u_{ab} should take the higher value of the capacitor branch voltage.

2) SCENARIO 2: S_2 CONDUCTS WHEN $u_{ab} \leq 0$

If thyristor S_2 conducts when $u_{ab} \leq 0$. At this time, the first-stage circuit is in the *RL* renewal time segment, and when capacitor C_2 starts to discharge, u_{ab} will change to a positive, and each crowbar diode will suddenly cut off. The current flow direction before and after the moment t_2 is shown in Fig. 4.

As shown in Fig. 4, the sudden change of u_{ab} causes a change in the flow direction of the current, so the calculation equation of the circuit will also be different. Neither the renewal current nor the discharge current of capacitor C_2 will charge the negative terminal of the already discharged capacitor C_1 during time segment $t_2 \sim t_3$. This is because the charged energy is released immediately.

Since both diode and thyristor have single-channel characteristics, the discharge of the capacitor C_2 will further increase the already existing current in the coil. A distributed feeder circuit during time segment $t_2 \sim t_3$ can be equated to the 2nd stage pulse discharge unit operating alone, where the initial current $i(t_2)$ of the coil is not 0, and the initial voltage $u(t_2)$ of the capacitor C_2 is not 0. The current in the circuit can be calculated using the principle of superposition. Note that the initial current in the excitation coil charges the negative terminal of the capacitor C_2 that is being discharged, and the voltage u_{C2} of the capacitor is actually the voltage difference between the positive and negative terminals. Therefore, the current of the excitation coil is the sum of the renewal current and the capacitor discharge current, while the voltage of the capacitor C_2 is the difference between the discharge voltage and the negative charging voltage, and the calculation equations are respectively

$$\begin{cases} i_L(t) = \int_{t_2}^{t} \left(\begin{array}{l} C_2 \left(R_{\text{total}} + \frac{\mathrm{dL}(x,i_L)}{\mathrm{dt}} \right) \frac{\mathrm{du}_{C2}}{dt} \\ + u_{C2} - \left(\frac{\mathrm{dL}(x,i_L)}{\mathrm{dt}} + R_L \right) i_L \end{array} \right) \frac{1}{L(x,i_L)} \mathrm{dt} + i(t_2) \\ u_{C2}(t) = -C_2 \left(R_{\text{total}} + \frac{\mathrm{dL}(x,i_L)}{\mathrm{dt}} \right) \frac{\mathrm{du}_{C2}}{\mathrm{dt}} \\ \qquad -C_2 L(x,i_L) \frac{d^2 u_{C2}}{\mathrm{dt}^2} - \frac{1}{C_2} \int_{t_2}^{t} i_L \mathrm{dt} \end{cases} . \tag{13}$$

where $R_{\text{total}} = R_{C2} + R_L$, and the voltage u_{ab} in the branch of the renewable diode can be expressed as

$$u_{ab}(t) = u_{C2} - R_{C2} i_{C2}. \tag{14}$$

The computational procedure of the 3rd stage to the nth stage of the multistage pulse discharge process is the same as that for the 2nd stage, and the computational equations are selected accordingly to the conduction of the thyristors at each stage and the circuit switching condition u_{ab}. If the thyristor conducts with $u_{ab} > 0$ and the circuit is switched by *RLC* then the calculation for scenario 1 is selected. Conversely, if the circuit is switched by *RL* when the thyristor conducts $u_{ab} \leq 0$ then the calculation for scenario 2 is selected. The flow chart of the time-segmented calculation method of the excitation current divided into time segments according to the on-going and circuit switching conditions of

the thyristors is shown in Fig. 5, where the 3rd stage to the nth stages are the same as the 2nd stage and are omitted.

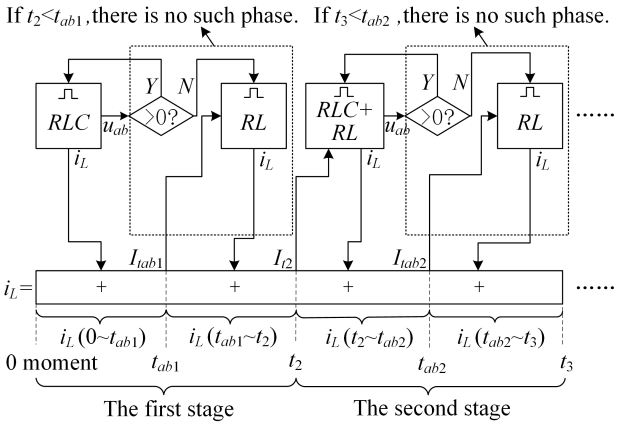

FIGURE 5. Flow chart of the time-segmented calculation method.

As shown in Fig. 5, the multistage pulse discharge process can be divided into an ordered combination of multiple time segments. At the switching time point $t_2, t_3 \ldots t_n$ of each thyristor conduction. In scenario 1 the residual voltage data in the capacitor is recorded and transferred. If scenario 2 then record and pass the residual current data in the coil. The latter time segment is calculated using the residual data transmitted in the previous time segment as the initial value, and the total current throughout the launch is the superposition of the currents of the segments on the time axis.

In addition, since the equivalent inductance $L(x, i_L)$ is also closely related to the real-time position of the projectile, the current equation and the equation of motion of the projectile must be solved jointly. When the launching process of reluctance coil launcher is analyzed using the imaginary displacement method, since the equivalent inductance is specifically denoted as $L(x, i_L)$, its EM energy should be specifically denoted as

$$W = \frac{1}{2}L(x, i_L) \cdot i_L^2(t) \tag{15}$$

By deflecting (15) with respect to x, the EMF of the projectile along the coil axis is

$$F_{em}(t) = \frac{\mathrm{d}W}{\mathrm{d}x} = \frac{1}{2}\frac{\partial L(x, i_L)}{\partial x} \cdot i_L^2. \tag{16}$$

Simultaneous

$$F_{em}(t) = ma = m\frac{\mathrm{d}^2x}{\mathrm{d}t^2}. \tag{17}$$

Further derive as

$$x_r(t) = \frac{1}{2m}\int_0^t \int_0^t \frac{\partial L(x, i_L)}{\partial x} \cdot i_L^2 \mathrm{d}t\mathrm{d}t + x(0) \tag{18}$$

where m is the mass of the ferromagnetic projectile.

Referring to the method described in [34], the equivalent inductance that varies with the projectile position and current is obtained by the look-up table method in the calculation process, and the launching process data such as current, EMF, and projectile velocity, that vary with time can be obtained by the joint solution.

III. SIMULATION AND EXPERIMENTAL VERIFICATION

A. INTRODUCTION TO THE ANALYTIC AL MODEL

In this study, a computational model of time-segmented calculation method was constructed using MATLAB Simulink software, and its computational results were compared with the FEA results obtained from ANSYS EM software, along with experimental validation.

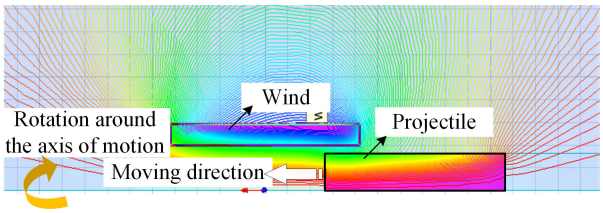

FIGURE 6. Projectile and coil in the experiment.

In this work, The FE simulation model is shown in Fig. 6. The projectile and coil used in the experiment are shown in Fig. 7, and the structural parameters of the projectile and coil are shown in Table 2.

TABLE 2. The structural parameters of the projectile and the coil.

Classification	Parameters	Value
Winding coil	Inner diameter (mm)	20
	Outer diameter (mm)	29
	Length (mm)	42
	Turn number	75
Projectile	Diameter (mm)	16
	Length (mm)	40
	Mass (g)	61.9
	Material	A3 steel

In order to implement the calculations using MATLAB/Simulink, 3D color mapping of the equivalent inductance and inductance gradient data table as a function of projectile position and excitation current is obtained according to the method of literature [34] as shown in Fig. 8.

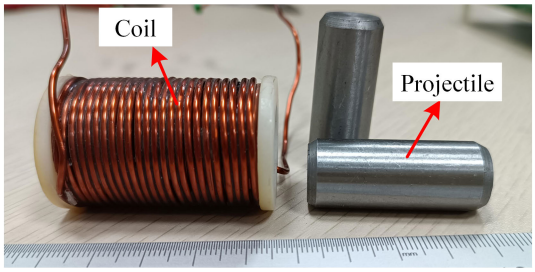

FIGURE 7. Projectile and coil in the experiment.

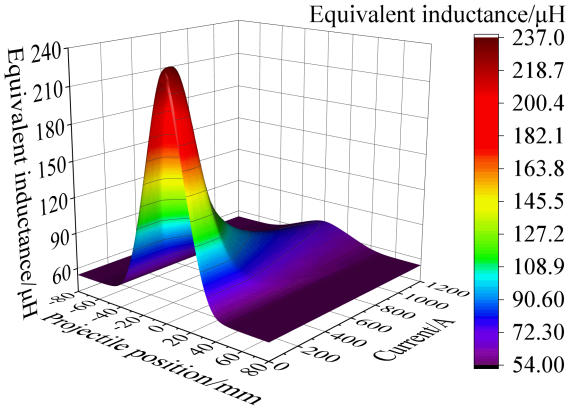

(a) The equivalent inductance data

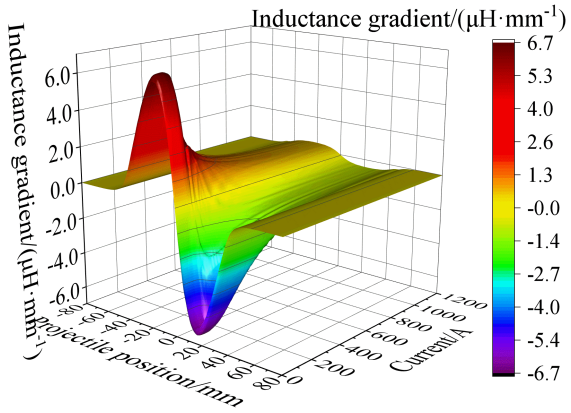

(b) The equivalent inductance gradient data

FIGURE 8. Equivalent inductance and inductance gradient data with changes in projectile position and excitation current.

As can be seen in Fig. 8, when the projectile coincides with the center of the coil, the equivalent inductance reaches a maximum value of about 237 μH. When the current in the coil exceeds about 200 A, the inductance decreases significantly. The minimum value of the equivalent inductance is about 54 μH, which is very close to the measured value of 55 μH at 1 kHz using a RCL bridge.

B. ACCURACY ANALYSIS OF THE TIME-SEGMENTED CALCULATION METHOL

In order to simplify the design and analysis process, each capacitor in the experimental device has the same specifications and is charged in parallel through the zero voltage switch (ZVS) booster. The overall experimental device of the reluctance coil launcher driven by the distributed feed method is shown in Fig. 9. The triggering circuit of the arbitrary thyristor is shown in Fig. 10, and each thyristor is connected in parallel at the output port of the microcomputer unit (MCU, model STM32F103C8T6), which is not described in the figure.

When the MCU detects that the transmit button is pressed, the microcontroller starts timing and uses the time delay program to trigger the gate of each thyristor in chronological order. The electrical parameters used in the distributed feeder

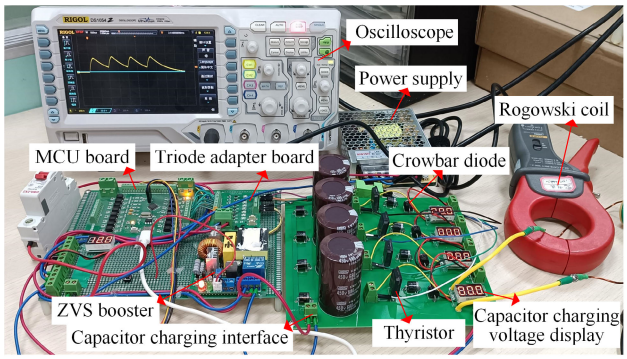

FIGURE 9. Integrated experimental device for reluctance coil launcher driven by distributed feeder circuit.

circuit driving experiment and simulation are shown in Table 3.

TABLE 3. Electrical parameters used in distributed feed transmission experiment and simulation.

Parameters	Symbol	1st satge	2nd stage	3rd stage	4th stage
Capacitance (μF)	C	680	680	680	680
Initial voltage (V)	$u_{C1}(0) \sim u_{C4}(0)$	300	300	300	300
Resistance (mΩ)	$R_{C1} \sim R_{C4}$	110	107	84	102
Trigger time (ms)	$t_1 \sim t_4$	0	1.0	2.0	3.0
Resistance (mΩ)	R_L		94		

The stray resistance R_C and the total coil branch resistance R_L of the pulse discharge units at each stage in Table 3 are obtained by parameter identification based on the measured current waveforms. The specific method of parameter identification is to make any stage of pulse discharge unit triggered individually to form a current in the absence of a projectile in the coil, and the sum of resistances R_C and R_L can be calculated in the RLC time segment based on the peak value of the current $i\left(t_{\text{peak}}\right)$ or the time of arrival of the current at the peak point t_{peak}. The calculation is given by

$$i\left(t_{\text{peak}}\right) = \frac{u_C(0)}{\omega L} \mathrm{e}^{-\sigma t_{\text{peak}}} \sin\left(\omega t_{\text{peak}}\right) \tag{19}$$

$$t_{\text{peak}} = \frac{1}{\omega} \arctan\left(\frac{\omega}{\sigma}\right) \tag{20}$$

$$\sigma = \frac{R_C + R_L}{2L}, \omega^2 = \frac{1}{LC} - \left(\frac{R_C + R_L}{2L}\right)^2 \tag{21}$$

where L is the inductance of the coil when it is hollow. R_L can be obtained by fitting the current waveform to the RL time segment, and the fitting equation is

$$i(t) = c \cdot \mathrm{e}^{-\frac{R_L}{L}t} \tag{22}$$

where R_L and c are the fitting parameters.

Since the four stages pulse discharge unit shares the same coil, the parameter identification of R_L is similar. Since the resistance of the coil is included in R_L, the parameter identification value of R_L is slightly larger than the measured resistance of the coil of 55 mΩ tested by a RCL bridge.

When the initial launch position $x(0)$ of the projectile is -33.7 mm, a comparison of the time-dependent launch process data obtained from the experimental, FEM, and the MATLAB/Simulink program of the time-segmented computational method is shown in Fig. 11. Among them, the EMF and the velocity of the projectile are difficult to be measured, and only the results of the FEM are compared.

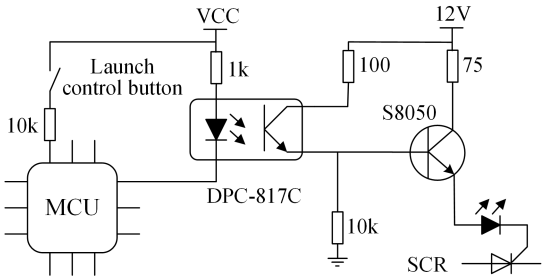

FIGURE 10. Trigger circuit for each thyristor.

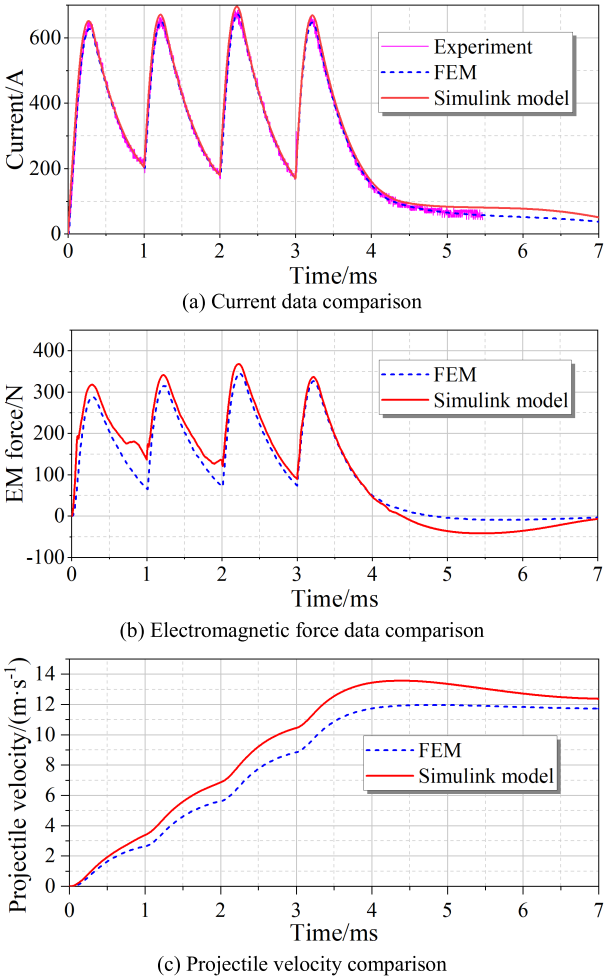

(a) Current data comparison

(b) Electromagnetic force data comparison

(c) Projectile velocity comparison

FIGURE 11. The time-varying launch process data obtained by experiment, finite element method and MATLAB/Simulink program are compared.

As can be seen from Fig. 11, the current calculated by the time-segmented calculation method is basically similar to the current waveforms obtained from experiment and FEM. However, the errors of EMF and projectile velocity are slightly larger, the main reason of which is explained with reference to the trend of inductance data in Fig. 8. As the pulse current during the launching process is mainly concentrated in the range of 200∼600 A, which is in the region where the trend of the equivalent inductance changes faster, and thus the equivalent inductance value will be significantly deviated by a slight difference in the current, especially when the projectile is closer to the excitation coil. From (18), it can be seen that the equivalent inductance deviation will lead to larger EMF and velocity deviation, while the current waveform is less affected by the inductance error.

Under transient launching conditions, the slower the projectile's motion, the longer the duration of this error, and the easier it is to accumulate the EMF and velocity errors. Therefore, it can be inferred that when the launch energy is raised, the deep magnetic saturation will make the equivalent inductance stabilize, the deviation will be reduced, and the speed of the projectile will be faster, so the accuracy of the time-segmented calculation method is higher.

C. DISTRIBUTED FEEDER CIRCUIT DRIVING METHOD FOR LAUNCH PERFORMANCE ENHANCEMENT

The data of the launching process in the case of single capacitor feeding and distributed feeding are obtained and compared by finite element simulation, respectively. In order to equalize the total energy of the two feeding methods, the capacitance value of the single capacitor is $4C = 2.72$ mF, the discharge voltage of the capacitor is also 300V, and the capacitor branch resistance is taken to be the mean value of 101 mΩ for $R_{C1} \sim R_{C4}$. A comparison of the current, equivalent inductance, EMF and velocity data obtained by FEM is shown in Fig. 12.

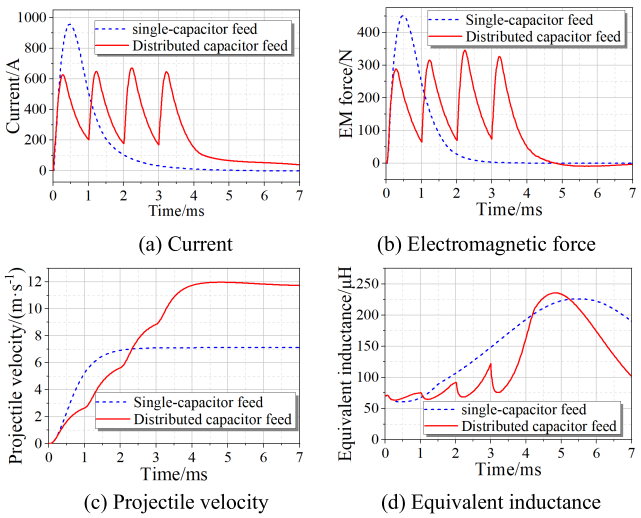

(a) Current

(b) Electromagnetic force

(c) Projectile velocity

(d) Equivalent inductance

FIGURE 12. Comparison of launch process data for single-capacitor feed and distributed capacitor feed.

As shown in Fig. 12(a), the current peak during single capacitor discharge is about 960 A, while none of

TABLE 4. The methods and results of this work to enhance the efficiency of single-stage reluctance coil launcher.

Researcher	Methods of efficiency improvement	Mass of the projectile (g)	Material of the projectile	Muzzle velocity (m/s)	Pre-optimization efficiency (%)	Optimized efficiency (%)	Efficiency gains (%)
This work	Distributed feed circuit is used to reduce the influence of magnetic saturation	61.9	Steel (A3)	11.72	1.301	3.535	171.7

the four current peaks of the distributed feeding method exceeds 670 A, which can be further reduced by increasing the number of capacitors. The magnetic saturation problem is weakened when the current peak is reduced, and thus the launch efficiency can be improved. As shown in Fig. 12(c), the muzzle velocity of the projectile when driven by a single capacitor discharge is 7.11 m/s, while the muzzle velocity of the projectile when driven by utilizing the distributed feed method is 11.72 m/s. By optimizing the trigger timing and other measures, the distributed feeder circuit driving method can be more efficient, especially for driving heavy projectiles with slow start-up speeds. The effect of replacing the traditional circuit with a distributed feed circuit is shown in Table 4.

IV. CONCLUSION

Reluctance coil launchers typically launch with high peak pulse currents, and the projectile is inefficient due to deep magnetic saturation. To address this problem, this paper proposes a method to utilize distributed feeder circuit for driving reluctance coil launchers in order to reduce peak current, suppress magnetic saturation and improve efficiency. Meanwhile, the reduction of peak current also helps to control the size and manufacturing cost of components.

The study includes two main aspects, one is to study the impact of this driving method on the launch performance and analyze the reasons. In the study when using a single capacitor for launching the efficiency is only 1.301%, which improved to 3.535% using the distributed feeder circuit driving method. The other is a proposal to calculate the time-varying data in the launching process through the time-segmented calculation method, which calculates accurate time-varying current data, but there are deviations in the EMF and projectile velocity curves. In subsequent studies, attempts will be made to combine the distributed feeder circuit driving method with other methods of improving efficiency to try to obtain more desirable results.

REFERENCES

[1] G. Fan, Y. Wang, K. Hou, Y. Miao, Y. Hu, and Z. Yan, "Research on energy conversion efficiency of the reconfigurable reconnection electromagnetic launcher," *Energy*, vol. 215, Jan. 2021, Art. no. 119088.

[2] L. Dong and S. Li, "Multipole field reconnection electromagnetic launcher," *IEEE Trans. Plasma Sci.*, vol. 46, no. 2, pp. 458–462, Feb. 2018.

[3] H. Deng, Y. Wang, and Z. Yan, "Study on the influence of armature on the efficiency of reluctance accelerator," *Def. Technol.*, vol. 18, no. 2, pp. 293–304, Feb. 2022.

[4] S. Guan, X. Guan, B. Wu, and J. Shi, "Analysis of the influence of system parameters on launch performance of electromagnetic induction coil launcher," *Energies*, vol. 15, no. 20, p. 7803, Oct. 2022.

[5] M. Wang and Z. Fu, "A new method of nonlinear causality detection: Reservoir computing Granger causality," *Chaos, Solitons Fractals*, vol. 154, Jan. 2022, Art. no. 111675.

[6] M. Lu, J. Zhang, and X. Yi, "A reverse electromagnetic force suppression circuit and its control method for reluctance coil-gun," *IEEE Trans. Plasma Sci.*, vol. 51, no. 4, pp. 1196–1203, Apr. 2023.

[7] Z. Li, Y. Shen, H. Li, and L. Song, "Study of the influence of electrical parameters on launch performance of projectile from the single-stage reluctance coil launcher," *J. Phys., Conf.*, vol. 1507, no. 8, Apr. 2020, Art. no. 082035.

[8] Z. Li, J. Wang, and X. Zhang, "The application of electromagnetic coil launching technology in non-war military operations AC machines," in *Proc. 16th Annu. Conf. China Electrotech. Soc. (CES)*, vol. 890, Apr. 2022, pp. 42–49.

[9] W. Huang, S. Huan, and Y. Xiao, "A miniature Hopkinson experiment device based on multistage reluctance coil electromagnetic launch," *Rev. Sci. Instrum.*, vol. 88, p. 9, Sep. 2017, Art. no. 094703.

[10] H. Liu, H. Nie, C. Zhang, and Y. Li, "Loading rate dependency of Mode I interlaminar fracture toughness for unidirectional composite laminates," *Compos. Sci. Technol.*, vol. 167, pp. 215–223, Oct. 2018.

[11] Z. Cao and Y. Zuo, "Electromagnetic riveting technique and its applications," *Chin. J. Aeronaut.*, vol. 33, no. 1, pp. 5–15, Jan. 2020.

[12] C. Weddeling, O. K. Demir, P. Haupt, and A. E. Tekkaya, "Analytical methodology for the process design of electromagnetic crimping," *J. Mater. Process. Tech.*, vol. 222, pp. 163–180, Aug. 2015.

[13] B. Zhu, J. Lu, J. Wang, and S. Xiong, "A compulsator driven reluctance coilgun-type electromagnetic launcher," *IEEE Trans. Plasma Sci.*, vol. 45, no. 9, pp. 2511–2518, Sep. 2017.

[14] V. Gies and T. Soriano, "Modeling and optimization of an indirect coil gun for launching non-magnetic projectiles," in *Proc. MDPI*, May 2019, vol. 8, no. 2, p. 39.

[15] M. Einat and Y. Orbach, "A multi-stage 130 m/s reluctance linear electromagnetic launcher," *Sci. Rep.*, vol. 13, no. 1, p. 218, Jan. 2023.

[16] J. L. Rivas-Camacho, M. Ponce-Silva, and V. H. Olivares-Peregrino, "The ringer as an inductive power source for a reluctance accelerator," *IEEE Trans. Plasma Sci.*, vol. 47, no. 5, pp. 2275–2281, May 2019.

[17] C. Liang, H. Xiang, X. Yuan, Z. Qiao, and Q.-A. Lv, "Reverse force suppression method of reluctance coil launcher based on consumption resistor," *IEEE Access*, vol. 9, pp. 62770–62778, 2021.

[18] T. S. El-Hasan, "Design of a single stage supersonic reluctance coilgun (RCG)," in *Proc. IEEE Pulsed Power Conf.*, Jun. 2011, pp. 964–969.

[19] S. J. Lee, J. H. Kim, and S. H. Kim, "Design and experiments of multi-stage coil gun system," *J. Vibroeng.*, vol. 18, no. 4, pp. 2053–2060, Jun. 2016.

[20] K. Leubner, R. Laga, and I. Dolezel, "Advanced model of electromagnetic launcher," *Adv. Electr. Electron.*, vol. 13, no. 3, pp. 223–229, Sep. 2015, doi: 10.15598/aeee.v13i3.1419.

[21] Y. Orbach, M. Oren, A. Golan, and M. Einat, "Reluctance launcher coil-gun simulations and experiment," *IEEE Trans. Plasma Sci.*, vol. 47, no. 2, pp. 1358–1363, Feb. 2019.

[22] T. Barrera and R. Beard, "Exploration and verification analysis of a linear reluctance accelerator," in *Proc. 17th Int. Symp. Electromagn. Launch Technol.*, Jul. 2014, pp. 1–6.

[23] H. Deng, Y. Wang, F. Lu, and Z. Yan, "Optimization of reluctance accelerator efficiency by an improved discharging circuit," *Def. Technol.*, vol. 16, no. 3, pp. 662–667, Aug. 2020.

[24] J. Zhao, H. Li, B. Zhao, J. Liu, L. Kong, and P. Zhang, "An improved pulsed power supply circuit for reluctance electromagnetic launcher based on bridge-type capacitor circuit," *IEEE Trans. Plasma Sci.*, vol. 51, no. 5, pp. 1351–1356, May 2023.

[25] M. M. M. Abdo, H. El-Hussieny, T. Miyashita, and S. M. Ahmed, "Design of a new electromagnetic launcher based on the magnetic reluctance control for the propulsion of aircraft-mounted microsatellites," *Appl. Syst. Innov.*, vol. 6, no. 5, p. 81, Sep. 2023.

[26] V. Sari, "Effect of change of reluctance launcher parameters on projectile velocity," *IEEE Access*, vol. 11, pp. 90027–90037, 2023.
[27] Y. Wen, L. Dai, and F. Lin, "Effect of geometric parameters on equivalent load and efficiency in rectangular bore railgun," *IEEE Trans. Plasma Sci.*, vol. 49, no. 4, pp. 1428–1433, Apr. 2021.
[28] S. Ma, X. Yu, and Z. Li, "Parameter analysis and optimized configuration of the PFU for inductive storage systems," *IEEE Trans. Plasma Sci.*, vol. 43, no. 5, pp. 1491–1496, May 2015.
[29] S. V. Bobashev, B. G. Zhukov, R. O. Kurakin, S. A. Ponyaev, and B. I. Reznikov, "An electromagnetic railgun accelerator: A generator of strong shock waves in channels," *Tech. Phys. Lett.*, vol. 40, pp. 1003–1006, 2014.
[30] Z. Wang, C. Shi, X. Zhang, X. Gao, S. Zhang, L. Huang, and J. Zhu, "Calculation of transient long pulse maximum current for CRAFT multi-parallel thyristor converters," *Fusion Eng. Des.*, vol. 188, Mar. 2023, Art. no. 113417.
[31] V. P. Kumar, S. Swarup, S. Rajput, G. Kumar, A. P. Nomula, K. B. Jadhav, S. Y. Taral, K. J. Daniel, and S. Datar, "Design and development of 4-MJ capacitor bank-based pulsed power system for electromagnetic launcher," *IEEE Trans. Plasma Sci.*, vol. 47, no. 3, pp. 1681–1689, Mar. 2019.
[32] B. A. Reinholz and R. J. Seethaler, "Design and validation of a variable reluctance differential solenoid transducer," *IEEE Sensors J.*, vol. 19, no. 23, pp. 11063–11071, Dec. 2019.
[33] Z. Yadong, G. Yujia, X. Min, B. Quanshun, N. Xiaobo, and L. Xiaolong, "Research on driving circuit improvement of coilgun," *IEEE Trans. Plasma Sci.*, vol. 47, no. 5, pp. 2222–2227, May 2019.
[34] M. Lu, J. Zhang, X. Yi, and Z. Zhuang, "Advanced mathematical calculation model of single-stage RCG," *IEEE Trans. Plasma Sci.*, vol. 50, no. 4, pp. 1026–1031, Apr. 2022.

MENGKUN LU was born in Xiaogan, Hubei, China, in 1989. He received the B.S. degree in automation of mechanical design and manufacturing and the M.S. degree in precision instruments and machinery from Hubei University of Technology, Wuhan, China, in 2011 and 2016, respectively, and the Ph.D. degree in electrical engineering from the Naval University of Engineering, Wuhan, in 2023. He is currently a Lecturer with Hubei Engineering University, Xiaogan. His research interest includes electromagnetic kinetic energy technology.

XIANGLIE YI was born in Yichun, China. He received the B.S. degree in automation of power systems, the M.S. degree in marine engineering, and the Ph.D. degree in marine engineering from the Naval University of Engineering, Wuhan, China, in 2004, 2007, and 2016, respectively. He is currently a Lecturer with the Naval University of Engineering.

ZHIFANG YUAN received the Ph.D. degree in electrical engineering from the Naval University of Engineering, in 2015. He has worked on the structure of motor design and motor control. He is currently a Lecturer with the Naval University of Engineering.

WEI GAO was born in Zibo, Shandong, in 1980. He received the Ph.D. degree in electrical engineering from the Naval University of Engineering, Wuhan, China, in 2011. He worked in the post-doctoral research station with the 28th Research Institute of Electronic Technology Group and was a Lecturer with the Naval University of Engineering. His research interests include wireless power transmission and electrical machinery and appliances.